Applied Surface Science 616 (2023) 156490

Contents lists available at ScienceDirect

Applied Surface Science

journal homepage: www.elsevier.com/locate/apsusc

Full Length Article

Effect of a water film on the material removal behavior of Invar during chemical mechanical polishing

Wan Wang [a], Dongpeng Hua [a], Qing Zhou [a,*], Shuo Li [a], Stefan J. Eder [b,c,*], Junqin Shi [a,*], Zhijun Wang [a], Haifeng Wang [a], Weimin Liu [a,d]

[a] State Key Laboratory of Solidification Processing, Center of Advanced Lubrication and Seal Materials, Northwestern Polytechnical University, Xi'an, Shaanxi 710072, PR China
[b] AC2T research GmbH, Viktor-Kaplan-Straße 2/C, 2700 Wiener Neustadt, Austria
[c] Institute for Engineering Design and Product Development, TU Wien, Lehárgasse 6 – Objekt 7, 1060 Vienna, Austria
[d] State Key Laboratory of Solid Lubrication, Lanzhou Institute of Chemical Physics, Chinese Academy of Sciences, Lanzhou 730000, PR China

ARTICLE INFO

Keywords:
Chemical mechanical polishing
Water film
Molecular dynamics simulation
Surface roughness
Subsurface damage

ABSTRACT

Understanding polishing mechanisms in water-lubricated environments has an important guiding value for surface engineering of precision devices. This work reveals the chemical mechanical polishing (CMP) mechanism of the Invar alloy under water lubrication by use of molecular dynamics simulation. The results show that the appropriate thickness of the water film and polishing speed can significantly reduce the surface roughness of the work piece and eliminate subsurface defects. With the increasing rolling speed, the variation of the surface roughness and subsurface damage thickness exhibits a trend of slowly decreasing and then reaching stability. In addition, with an increase in water film thickness, more defects were formed in the subsurface region due to greater surface stresses, although the roughness could be reduced due to an increase of passivated atoms on the work piece surface. These results would be helpful for understanding the CMP mechanism under water-lubricated conditions and for promoting the development of surface engineering for micro/nano components.

1. Introduction

With the rapid development of ultra-precision manufacturing technology, chemical mechanical polishing (CMP) has been widely used due to its ability to achieve global and local surface planarization [1,2]. CMP utilizes the synergy of mechanical and chemical actions to achieve material removal at the atomic scale, helping to produce smooth and defect-free surfaces [3,4]. Among them, the factors affecting the final performance of CMP mainly focus on the interaction between the work piece surface and the slurry/abrasives [5–8]. During the polishing process, the motion state of the abrasives is difficult to control, and these abrasives will cause two-body or three-body wear on the surface of the work piece [3]. The polishing slurry plays an important role in changing the tribological properties between the abrasives and the work piece [9]. Therefore, studying the mechanical and corrosive wear induced by the abrasives and the slurry is of great significance for understanding the physical or chemical mechanisms in CMP, which can help us to optimize polishing methods at the nanoscale.

In order to obtain defect-free surfaces and improve polishing efficiency, researchers have conducted extensive research on the abrasive wear process and the effect of polishing slurry [10–15]. Studies have shown that the abrasives are subjected to shear stress and normal stress during the polishing process, which leads to sliding and rolling motion. The sliding abrasives are conducive to material removal, while the rolling abrasives can reduce the friction coefficient [16]. The effect of the slurry on the polishing process is more complicated: water, as the main and fundamental component of polishing slurry, has a positive effect on improving the surface quality of the work piece and reducing abrasive wear [17]. However, in a water-lubricated polishing process, the removal of material by abrasives is complicated because it partially takes place on the nano scale, and it is difficult to observe nanoscale deformation processes of materials in experiments.

The polishing process, considered at the atomic level using molecular dynamics (MD) simulations, has been extensively studied [18–21]. However, these studies usually treat the abrasives as a rigid body without any rolling motion, which is inconsistent with the abrasive motion during actual polishing [16]. Therefore, many researchers combine sliding and rolling motions to explain the surface processing

* Corresponding authors.
E-mail addresses: zhouqing@nwpu.edu.cn (Q. Zhou), stefan.eder@ac2t.at (S.J. Eder), junqin.shi@nwpu.edu.cn (J. Shi).

https://doi.org/10.1016/j.apsusc.2023.156490
Received 27 October 2022; Received in revised form 10 January 2023; Accepted 16 January 2023
Available online 20 January 2023

mechanism. For example, Nguyen et al. [22–24] revealed the wear mechanism of sliding motion and rolling motion at various infeed depths, and found that during the rolling process, the deformation behavior of the work piece depends on the ratio between the rolling speed and the sliding speed. Meng et al. [25] found that the wear mechanism depends on the abrasive rolling speed, in which the material removal mechanism changes from the cutting state to the plowing state as the abrasive rotational speed increases.

At present, the research on the mechanism of the effect of water on the polishing behavior of abrasive particles is being considered, but still very limited. Shi et al. [26] investigated the material removal mechanism of single crystal copper at the atomic scale and found that the monolayer atom removal is influenced by the adhesion between water and copper atoms. The resulting machined surface is relatively smooth, and the subsurface damage is free from plastic defects. Tian et al. [27] studied the effect of a water film on the nano-friction behavior of a Cu/Ag bilayer film and found that the presence of the water film aggravated the subsurface damage and dislocation nucleation at the interface, but significantly improved the groove surface quality. Li et al. [28] investigated the effect of a water environment on the polishing process of single crystal lutetium oxide. The study showed that the water environment is beneficial to ductile mode removal of material from the sample, reducing the tensile stress concentration area and brittle damage below the work piece surface. Clearly, MD simulations have unique advantages in studying the patterns of abrasive motion and the effect of water molecules on material deformation and damage at the nanoscale. Studying the role of water in CMP can also provide basic guidance to further explore the complex occurring chemical reactions.

The Invar alloy ($Fe_{65}Ni_{35}$) is widely used as a unique low expansion coefficient alloy [29–31], but its low strength, low hardness and active chemical properties make it highly likely to generate subsurface damage, deformation, and dislocations during processing [32]. Therefore, in this work we have selected Invar to study its two-body and three-body polishing mechanisms under water lubrication conditions. The material removal behavior of the abrasive is considered under two different forms of motion (sliding and rolling). The atomic wear process and subsurface damage mechanism of dry polishing and water-lubricated polishing at various infeed depths are discussed. On this basis, a comprehensive and direct observation of the atomic removal process at several rolling speeds in water-lubricated polishing was carried out, and the effect of water on the surface and subsurface quality was investigated. Compared with previous work [33], this work focuses on the effect of water on the removal process of surface atoms and on the subsurface damage mechanism to obtain a machined surface of high quality. This will help reveal the role of water in the CMP process and understand the friction and wear properties of the material.

2. Methodology

The reliability of an MD simulation mainly relies on the accuracy of the interaction potential. There were four kinds of atomic interactions in the MD simulations at hand. The interactions between Fe and Ni atoms were represented by the second nearest-neighbor modified embedded-atom-method (2NN MEAM) potential [34]. As the hardness of abrasives in real polishing processes is much greater than that of the work piece, and the deformation of the abrasives in polishing is negligible, the diamond abrasive was treated as a rigid body. Due to the limitations of potential functions and computational power, it is difficult to consider the complex chemical reactions and mechanical interactions among abrasive particles, substrates, and chemicals during CMP. Therefore, a simplified atomic-scale material removal model is proposed, which neglects other components of the polishing slurry and replaces it by a water film. The rigid TIP4P model [26,35] was applied to the water film. The interactions of H atoms in water molecules with other types of atoms were neglected due to their weak influence. Lennard-Jones potentials were adopted to describe interactions between C–Fe, C–Ni, O–Fe, and O–Ni with $\varepsilon_{C-Fe} = 0.12$ eV, $\sigma_{C-Fe} = 2.71$ Å, $\varepsilon_{C-Ni} = 0.12$ eV, $\sigma_{C-Ni} = 2.69$ Å, $\varepsilon_{O-Fe} = 0.06$ eV, $\sigma_{O-Fe} = 2.74$ Å, $\varepsilon_{O-Ni} = 0.06$ eV, and $\sigma_{O-Ni} = 2.72$ Å [36–38], and the cutoff distance was set to 7 Å.

The MD simulations in this work include three stages. The first stage was the relaxation of the initial system for 50 ps to minimize the system energy using the NVE ensemble and a Langevin thermostat. The abrasive center was located at 30 Å above the top surface of the work piece to prevent any interaction between the abrasive and the work piece (or water molecules) during relaxation as shown in Fig. 1(a). During relaxation, some work piece atoms are passivated by water molecules to form chemical bonds with oxygen atoms, a phenomenon that is also frequently observed in experiments [39,40]. We define the work piece atoms whose atomic distance is smaller than the bonding distance of Fe-O (2.02 Å) [41] and Ni-O (1.91 Å) [42] as passivated atoms [43]. For a water film thickness of 10 Å, the number of work piece atoms passivated after relaxation is 1336 as shown in Fig. 1(b). The second stage was the nanoindentation process, during which the abrasive vertically penetrated into the (0 0 1) surface of the work piece at a constant speed of 50 m s^{-1}. The abrasive completely penetrated the water film and then pressed into the work piece to a depth of 5 Å. Finally, the abrasive began polishing the work piece along the [1 0 0] direction at a sliding speed of 100 m s^{-1} as shown in Fig. 1(a). Various polishing depths h (0 Å and 5 Å), rolling speeds ω (50 m s^{-1}, 100 m s^{-1}, 150 m s^{-1}, and 200 m s^{-1}, which is equal to 3.98 rad/ns, 7.96 rad/ns, 11.94 rad/ns, and 15.92 rad/ns), and water film thicknesses H (0 Å, 5 Å, 10 Å, 15 Å, and 20 Å) were used to reveal the effect of the water molecules on the atomic removal behavior. The simulation data is analyzed using the visualization software of OVITO [44], which provides the dislocation extraction algorithm (DXA) [45].

3. Results

3.1. Effect of water molecules on material removal

Fig. 2 shows the atomic removal process for two cases of dry polishing and water-lubricated polishing with a water film thickness of 10 Å at polishing distances of 0, 30, and 40 Å. To better observe the work piece atom removal process, the work piece atoms with area 2×5 $Å^2$and their surrounding oxygen atoms are marked in green and dark blue, respectively. At a polishing depth of 0 Å (Fig. 2(a)), the work piece atoms in green adhere around the abrasive under dry conditions, indicating adhesive removal of work piece atoms. This reveals that there is an adhesion force between the abrasive and the metal surface atoms, which is because of the broken metal bonds of the work piece atoms after being impacted by the abrasive, resulting in the work piece atoms adhering to the trailing side of the abrasive.

However, the addition of water resulted in a distinct modification of the interactions between the abrasive atoms and the work piece atoms. On the one hand, the surface atoms of the work piece exhibit slight elastic deformation at the indentation, because the water molecules below the abrasive can transfer the loading force of the abrasive to the work piece surface [26]. On the other hand, the surface atoms of the work piece were passivated by some water molecules, so that the work piece atoms are closely combined with the surrounding oxygen atoms during the polishing process as shown in Fig. 1(b). The passivation eliminates the adhesion between the abrasive atoms and surface atoms of the work piece, resulting in a reduced material removal capability of the abrasive [46,47]. When the polishing depth is 5 Å (Fig. 2(b)), the material removal mechanism is characterized by significant adhesion and plowing in dry polishing, while only plowing exists in water-lubricated polishing. Therefore, the water film in polishing can passivate the surface of the work piece and effectively reduce the adhesion between the abrasive and the work piece.

Fig. 3 shows the top views of the worn configuration of the work piece surface at a polishing distance of 140 Å in dry polishing and water-lubricated polishing. Before polishing, the work piece was divided into

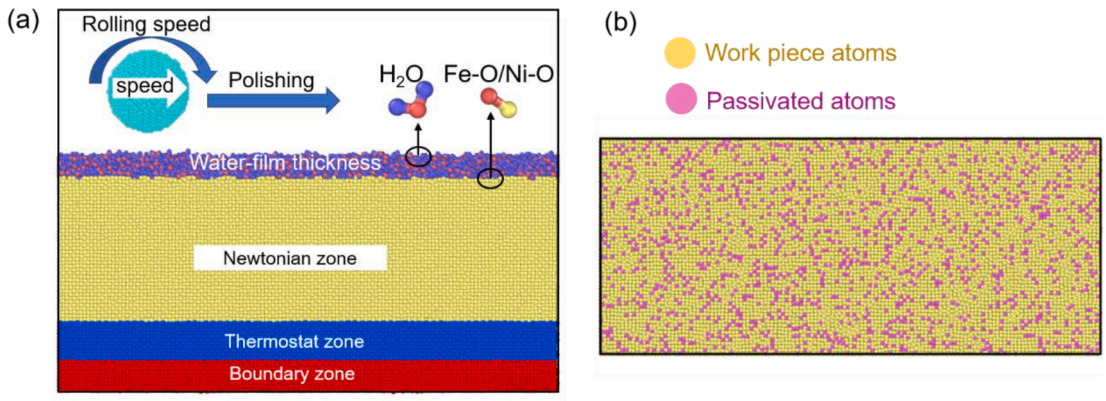

Fig. 1. (a) MD simulation model of the CMP of Invar covered with a water film, and (b) the passivated work piece surface.

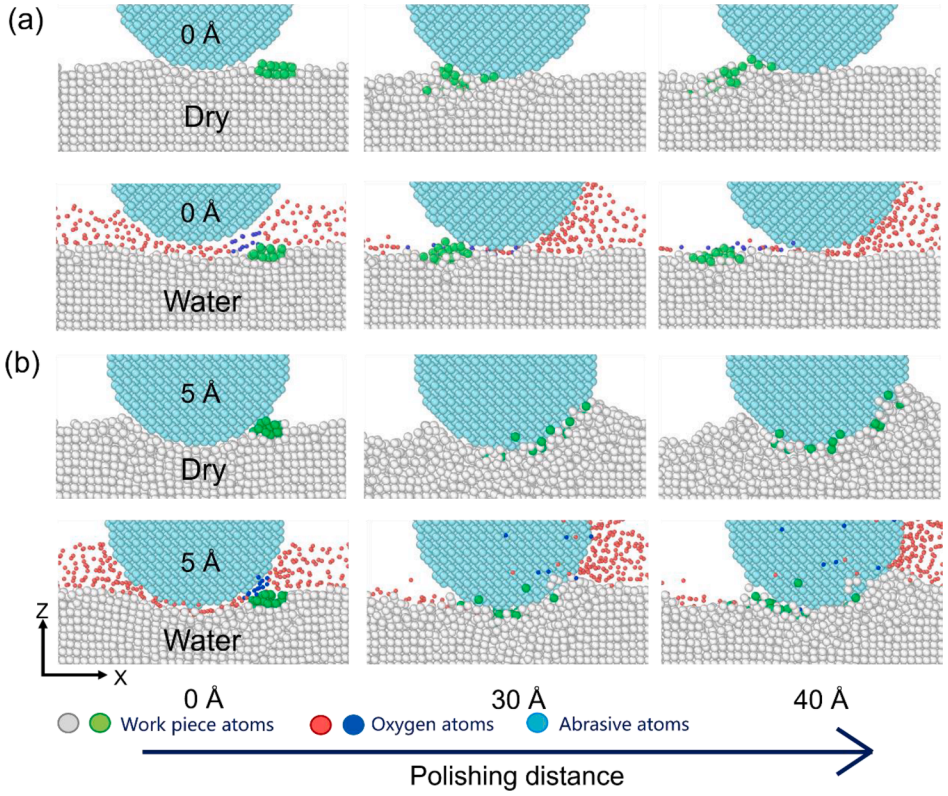

Fig. 2. Atomic removal process under dry polishing and water-lubricated polishing conditions within a 5 Å slice of the central polishing region after various polishing distances at a polishing depth of (a) 0 Å and (b) 5 Å (H = 10 Å). Color code: red, oxygen atoms in water molecule; cyan, abrasive; white, work piece atoms. To follow the atomic removal process in more detail, the work piece atoms in a small contact area are marked in green, and a small part of the oxygen atoms around it are marked in dark blue. (For interpretation of the references to color in this figure legend, the reader is referred to the web version of this article.)

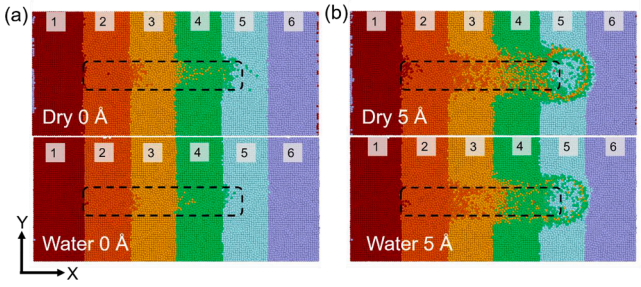

Fig. 3. Top views of the worn configuration of the polished surface at a polishing distance of 140 Å under dry and water-lubricated polishing with a polishing depth of (a) 0 Å and (b) 5 Å (H = 10 Å). The surface is separated into several zones marked by different colors, and the atomic removal and advection occur in 6 zones marked by numbers 1–6. The dashed black line marks the polishing contour.

several regions, marked with different colors and numbers 1–6. As can be seen from Fig. 3(a), when the polishing depth is 0 Å, some work piece atoms move forward from their original positions to the adjacent area due to the adhesion of the abrasive in dry polishing. However, there is almost no cross-regional movement of work piece atoms in water-lubricated polishing. At a polishing depth of 5 Å (Fig. 3(b)), due to the combined effect of adhesion and plowing, the work piece atoms show significant cross-regional atomic advection in dry polishing, while this phenomenon is much suppressed in water-lubricated polishing. In addition, the pile-up atoms (zone 5) in dry polishing contain many atoms from zones 2–4, whereas they are mainly from zone 4 (with a small number from zone 3) in water-lubricated polishing. This further proves that the passivation effect of the water film significantly reduces the adhesive wear of the work piece.

Fig. 4(a) shows the von Mises stress of the cross-section and top view of the work piece when the abrasive is at different positions. Before the translational motion of abrasive, there is no significant stress on the

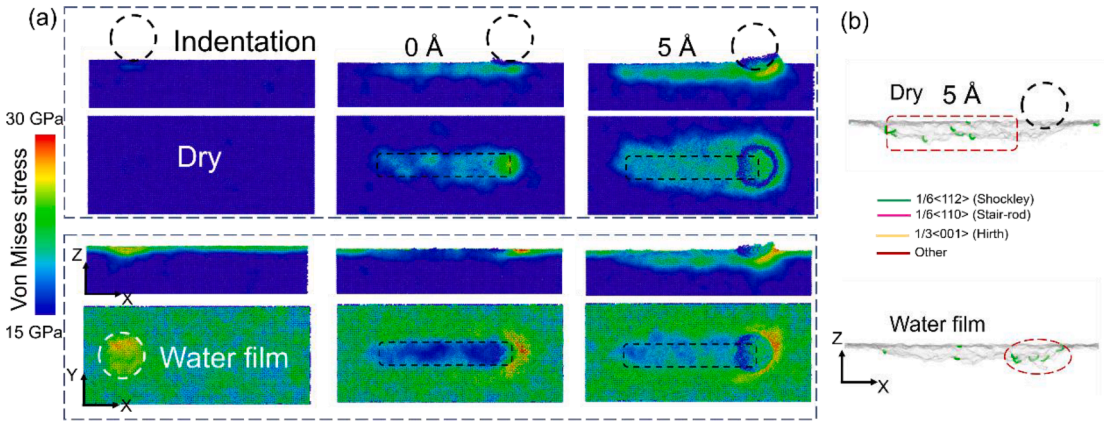

Fig. 4. (a) Von Mises stress distribution in the incipient contact between abrasive and work piece under dry polishing and water-lubricated polishing conditions at polishing depths of 0 and 5 Å, and (b) dislocation distribution under dry polishing and water-lubricated polishing conditions after a polishing distance of 140 Å at a polishing depth of 5 Å ($H = 10$ Å).

work piece surface under dry polishing, but a uniform compressive stress appears on the work piece surface in water-lubricated polishing [27], which can level the work piece surface. After some time of polishing (irrespective of the polishing depth), the stress mainly concentrates in the groove and beneath the abrasive under dry polishing, whereas it mainly concentrates in front of the abrasive in the water-lubricated polishing process.

Moreover, the distinct stress distribution during dry and water-lubricated polishing is closely related to the plastic deformation as reflected by the dislocation distribution. As shown in Fig. 4(b), the stress concentration in the groove region makes its dislocations mainly concentrate below the groove under dry polishing. By contrast, the stress concentration in front of the abrasive causes dislocation generation mainly in front of the abrasive in water-lubricated polishing. Besides, the atomic lattice of the work piece atoms is destroyed under the influence of stress, which would lead to a thicker amorphous layer on the ground surface under dry polishing [48]. Contrarily, the presence of water promotes an increase in heat dissipation during the polishing process, which decreases the energy available for a structural phase transition [49], leading to a decrease of the subsurface damage depth. Therefore, the existence of a water film does not only lead to lower surface roughness, but also reduces the damage thickness of subsurface layer.

During the polishing process, the relative motion between abrasive and work piece causes an increase in the system temperature, which could affect the polishing quality, including surface roughness and subsurface damage thickness [50–52]. Therefore, it is necessary to discuss the work piece temperature during polishing. Since the temperature increase of the work piece does not change significantly at a polishing depth of 0 Å, the temperature distribution of the work piece at a polishing depth of 5 Å in dry and water-lubricated polishing are shown in Fig. 5. It can be seen that the location where the abrasive touches the work piece exhibits an obvious temperature peak, and the heat-affected zone is wide in dry polishing. The thermal effect promotes severe plastic deformation, resulting in a rough work piece surface and more internal defects (see Fig. 4(b)). In a water-lubricated environment, however, the contact region between the abrasive and the work piece remains at a relatively low temperature because the water film aids heat dissipation. This heat dissipation facilitates the reduction of structural damage in the non-scratch area and high-temperature wear of the abrasive (see Fig. 4 (b)) [53].

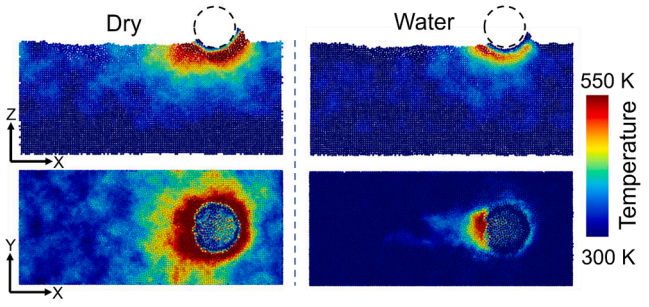

Fig. 5. Temperature distribution in the work piece under dry (left) and water-lubricated polishing (right) at a polishing depth of 5 Å ($H = 10$ Å).

3.2. Material removal process with a rolling abrasive

Through simulation, we found that when the abrasive moves in a pure sliding mode, it is difficult for water molecules to enter into the contact region between abrasive and work piece at large polishing depths, which is consistent with previous research on water-lubricated polishing [49,54]. However, in real polishing processes, it can be observed that the movement of the abrasives is characterized by both sliding and rolling motion, which may be controlled by varying the polishing load and/or the abrasive type [3,55]. Therefore, the sliding and rolling of the abrasive should be considered simultaneously in the simulation process. In the following, the water-lubricated polishing mechanism with a water film thickness of 10 Å was studied with abrasive rolling speeds of 50, 100, 150, and 200 m s^{-1} (i.e., 3.98, 7.96, 11.94 and 15.92 rad/ns), while the pure sliding speed of the abrasive was kept at 100 m s^{-1}.

Fig. 6 shows the atomic removal process at polishing distances of 60 Å, 80 Å, 90 Å, and 100 Å at various rolling speeds. Some central work piece atoms are colored green, the red frame marks their initial position, and the water molecules are not shown for better clarity. To better illustrate the atomic removal process in rolling motion, we have added the atomic removal process in pure sliding motion for comparison as shown in Fig. 6(a1)-(a4). It can be seen that the abrasive can easily remove the marked atoms from their original positions in a pure sliding way and pile them up in front of the abrasive. When the tangential rolling speed is smaller than the sliding speed, although the marked atoms are rolled under the abrasive by the abrasive rolling, the net speed of the contact point between abrasive and work piece remains positive in the $+X$ direction, resulting in the marked atoms still moving forward, as shown in Fig. 6(b1)-(b4). When the tangential rolling speed is equal to the sliding speed, the abrasive moves in a pure rolling way. The speed of the contact point between abrasive and work piece is zero, thus the marked atoms are only rolled under the abrasive without moving, as shown in Fig. 6(c1)-(c4). When the tangential rolling speed is greater than the sliding speed, the net speed of the contact point between the

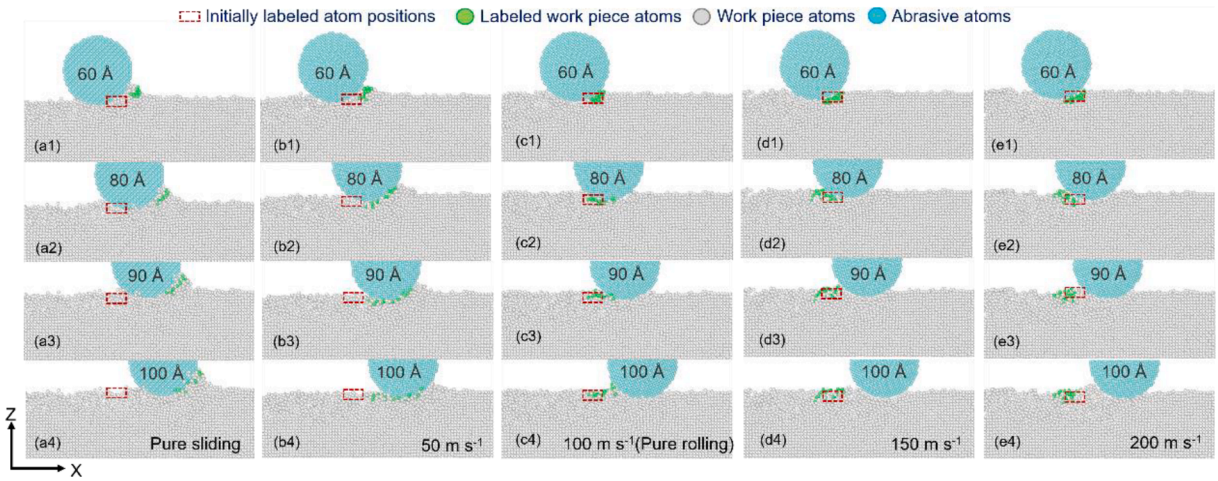

Fig. 6. Atomic removal process within a 5 Å slice in the polished center region at polishing distances of 60, 80, 90 and 100 Å with a rolling speed of (a1)-(a4) 0 m s^{-1}, (b1)-(b4) 50 m s^{-1}, (c1)-(c4) 100 m s^{-1}, (d1)-(d4) 150 m s^{-1}, and (e1)-(e4) 200 m s^{-1} ($H = 10$ Å, $h = 5$ Å). Color code: cyan, abrasive; white, work piece atoms. To follow the atomic removal process in more detail, a small number of work piece atoms are labeled in green, and the red frame line marks their initial position. The water molecules are not shown for clarity. (For interpretation of the references to color in this figure legend, the reader is referred to the web version of this article.)

abrasive and the work piece becomes negative in –*X* direction. Therefore, the marked atoms are not only rolled under the abrasive, but also moved backward, as shown in Fig. 6(d1)-(d4). With the increasing rolling speed, the marked atoms move farther backward, and the atomic pile-up appears behind the abrasive, as shown in Fig. 6(e1)-(e4).

To better observe the motion of the work piece atoms during polishing, we marked the work piece into 6 zones with different colors and numbers in the top view as shown in Fig. 7. The initial position of the abrasive is at the junction of the zones 1 and 2, and the final position is in the middle of zone 5. During the transition from the indentation stage to the scratch stage, the trailing half of the abrasive will lose contact [56], and the water film reduces the adhesion of the abrasive, so there is almost no transverse displacement of the atoms in zone 1. The migration ability of work piece atoms in other regions is consistent with the phenomena discussed in Fig. 6. With the increase of rolling speed, the speed of the contact point between the abrasive and the work piece changes from positive to negative along the *X* direction, thus the rolled work piece atoms change from forward motion to backward motion.

Fig. 8(a) shows the change in the number of water molecules in the groove and the top view of the distribution of water molecules at different rolling speeds. It can be seen that the number of water molecules in the groove increases with the increasing rolling speed, which can also be seen visually in the black box area of the illustration. Fig. 8 (b) shows the side views of the surface topography at rolling speeds of 50 m s^{-1} and 150 m s^{-1}, respectively. It can be seen that when the rolling speed is smaller than the sliding speed, the water molecules are squeezed out to the front of the abrasive and on both sides of the groove. When the rolling speed is greater than the sliding speed, the water molecules on the surface of the work piece can be entrained into the contact region between abrasive and work piece, and thereby water molecules can enter in the groove.

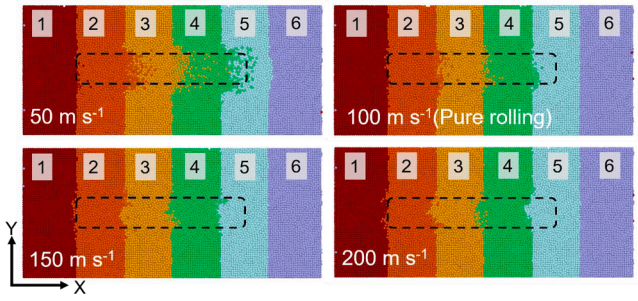

Fig. 7. Snapshots of the worn configuration of the top views of the polishing surface for various rolling speeds at a polishing distance of 140 Å ($H = 10$ Å, $h = 5$ Å). The surface is separated into several zones marked by different colors, and the atomic removal and shift occur in 6 zones marked by numbers 1–6. The black line marks the polishing contour.

To better illustrate the effect of passivation on the work piece surface, Fig. 9(a) shows the atomic surface passivation morphologies before and after polishing. It can be seen that before polishing, passivated atoms are scattered throughout the surface of the work piece. After the polishing process dominated by sliding, there remain almost no passivated atoms in the groove. After the polishing process dominated by rolling, some passivated atoms can be found in the groove. Fig. 9(b) illustrates the number of passivated atoms at various rolling speeds. The number of passivated atoms on the work piece surface is the same before indentation. After polishing, the number of passivated atoms is significantly reduced, because some passivated atoms are plowed away and a new, non-passivated groove surface is formed.

Fig. 9(c) shows the groove roughness after polishing at various rolling speeds. The roughness is calculated as the sum of the absolute value of the difference between the atomic height and the average height in the groove, and the error bars are obtained by calculating four different areas in the groove [33]. It can be seen that the increasing rolling speed helps to improve the groove surface quality. In general, the work piece deformation caused by abrasive sliding is almost uniform across the entire scratch area as shown in Fig. 6, because a sliding abrasive plows across the substrate, causing more atoms to gather in front of it. When the abrasive rolls, the pile-up atoms will be easily carried under the abrasive, resulting in a rough, deformed surface [57]. With the increase of rolling speed of the abrasive, atoms are directly rolled without experiencing pile-up, and the rolling abrasive can relieve shear force involved in sliding, so the roughness of the deformed surface decreases, which is consistent with the phenomenon observed in the experiment [58]. However, the roughness increases slightly at the rolling speed of 200 m s^{-1}, which is because there are more work piece atoms piled up behind the trailing end of the abrasive.

The shear stress distribution of the work piece at various rolling speeds is shown in Fig. 10(a). Two distinct regions of shear stress concentration can be observed during polishing. One is the compressive stress zone below the front of the abrasive, which is believed to be the main driver of pile-up behavior. The other is the tensile stress zone below the rear of abrasive, which will drive the defects in the subsurface region of the work piece to annihilate towards the surface [59,60]. With the increase of rolling speed, the change in direction of the force exerted

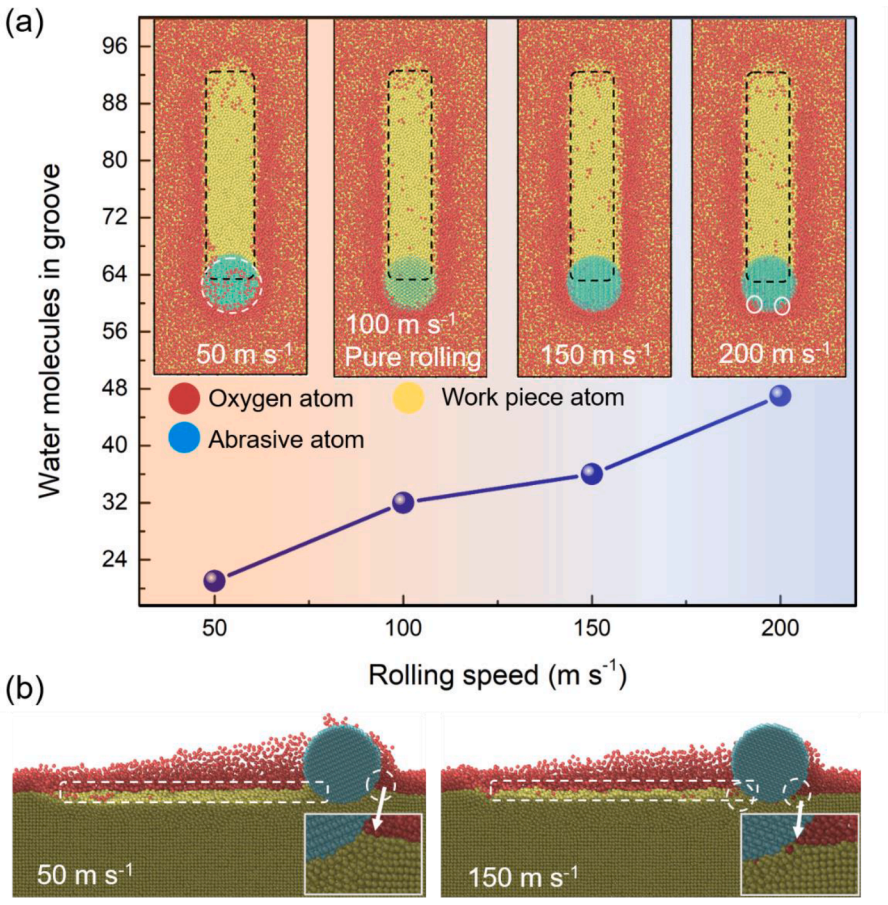

Fig. 8. (a) Distribution of water molecules in the groove at various rolling speeds, and (b) cross-sectional morphology at rolling speeds of 50 m s^{-1} and 150 m s^{-1} (H = 10 Å, h = 5 Å).

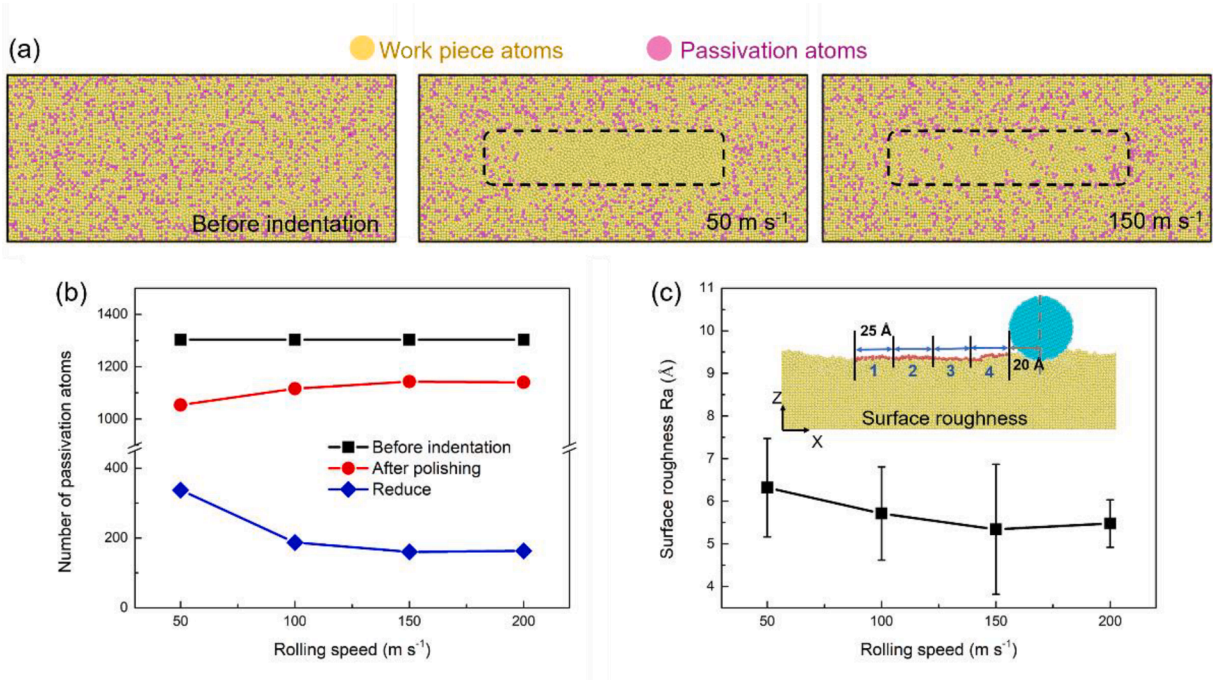

Fig. 9. (a) Surface passivation morphology before indentation and after polishing, (b) the number of passivated atoms, and (c) the surface roughness at different rolling speeds (H = 10 Å, h = 5 Å).

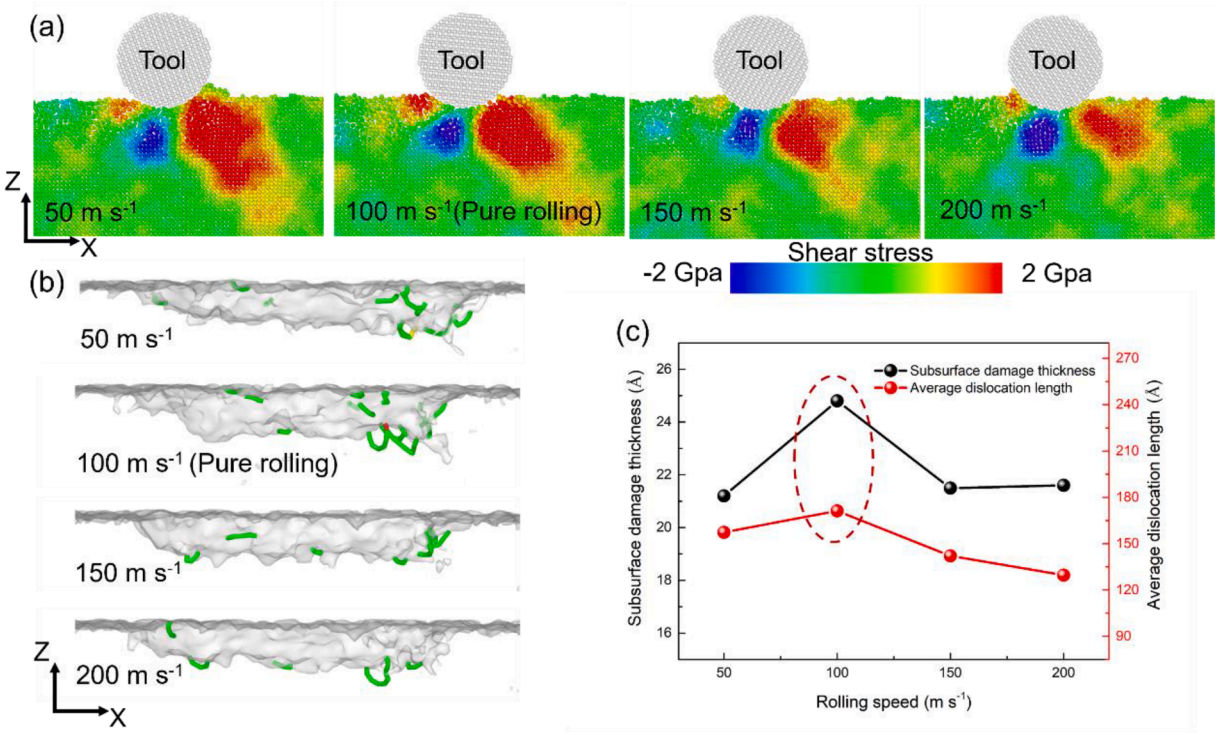

Fig. 10. (a) Shear stress distribution and (b) dislocation distribution of polishing distance 90 Å, and (c) curves of subsurface damage and average dislocation length at various rolling speeds ($H = 10$ Å, $h = 5$ Å).

by the abrasive on the region in contact with the work piece leads to the reduction of the compressive stress zone and the expansion of the tensile stress zone [61]. This change in the stress region would affect the activation of subsurface dislocations. Fig. 10(b) shows the dislocation distribution corresponding to the shear stress in Fig. 10(a). It can be seen that under the action of compressive stress, a large number of dislocations are generated in front of the abrasive. As the compressive stress range narrows, the number of dislocations in front of the abrasive decreases. The increase of the rolling speed increases the number of dislocations in the groove, which is the result of tensile stress pulling dislocations inside the work piece to the surface [62]. Fig. 10(c) presents the variation of the average dislocation line length and subsurface damage thickness at various rolling speeds. It can be seen that when the sliding speed is equal to the rolling speed (pure rolling), the subsurface damage of the work piece is the largest. This is because the abrasive moving in a pure rolling way compress the atoms on the surface toward the interior of the work piece, unlike in other motion forms, atoms partially pile up in front of or behind the abrasive, thus causing greater thickness of the subsurface damage layer.

3.3. *Effect of water film thickness on the rolling-induced subsurface damage*

The number of water molecules reflects the effect of the concentration of polishing slurry on the polishing process and influences the tribological properties of two contact surfaces in relative motion in the experiment [58,63], which has an important effect on the surface and subsurface region of the work piece. Therefore, this part we will consider a range of water film thicknesses (5 Å, 10 Å, 15 Å, and 20 Å) to conduct polishing simulations at a rolling speed of 150 m s^{-1}.

Before polishing, the abrasive is pressed into the work piece to a constant depth of 5 Å, and the participation of the water film will affect the subsequent polishing process. Fig. 11 (a)-(c) show the contact surface morphology, stress distribution and dislocation distribution of the work piece with various water film thicknesses in the indentation stage. As seen from Fig. 11 (a), the indentation area expands with the increase of the water film thickness. This is because the abrasive presses water molecules into the work piece during the indentation process. The thicker the water film, the more water molecules will be pressed in, and the larger the indentation area will be. This will also affect the stress distribution and dislocation morphology in the indentation region [57], as shown in Fig. 11 (b) and (c). When the water film is thin (5 Å), the stress distribution of the work piece still conforms to the Hertz contact theory [64,65], that is, the maximum stress occurs at a certain distance below the contact surface. Therefore, dislocations also nucleate from this region and concentrate below the contact region. With the increase of water film thickness, the maximum stress area gradually transfers from below the contact surface to the area surrounding the contact region, and the distribution is circular, which leads to the generation and distribution of a large number of dislocations around the contact region.

Fig. 12(a) shows the distribution of water molecules over the work piece regions defined earlier. When the water film thickness is 15 and 20 Å, a large number of water molecules are adsorbed around the abrasive and cover the surface of the abrasive during the polishing process. For the convenience of observation, slice processing is performed at the center of the abrasive as shown in Fig. 12(a). From the distribution of water molecules, it can be seen that the ability of the abrasive to remove water molecules in zone 1 is very weak, and the water molecules in zone 2 are mainly in the groove, which best reflects the lubrication effect of water during polishing. Fig. 12(b) shows the statistics of the number of water molecules below the abrasive at the end of indentation as well as the number of water molecules in the grooves after polishing for various water film thicknesses. It can be clearly seen that with the increase of the water film thickness, the number of water molecules below the indentation region and in the grooves increases with the increasing water film thickness. When the water film thickness is high, more water molecules in zone 2 will enter the groove during polishing. The water molecules left in the grooves can reduce the direct interaction between abrasive and work piece atoms to achieve the lubricating effect of the water film [36].

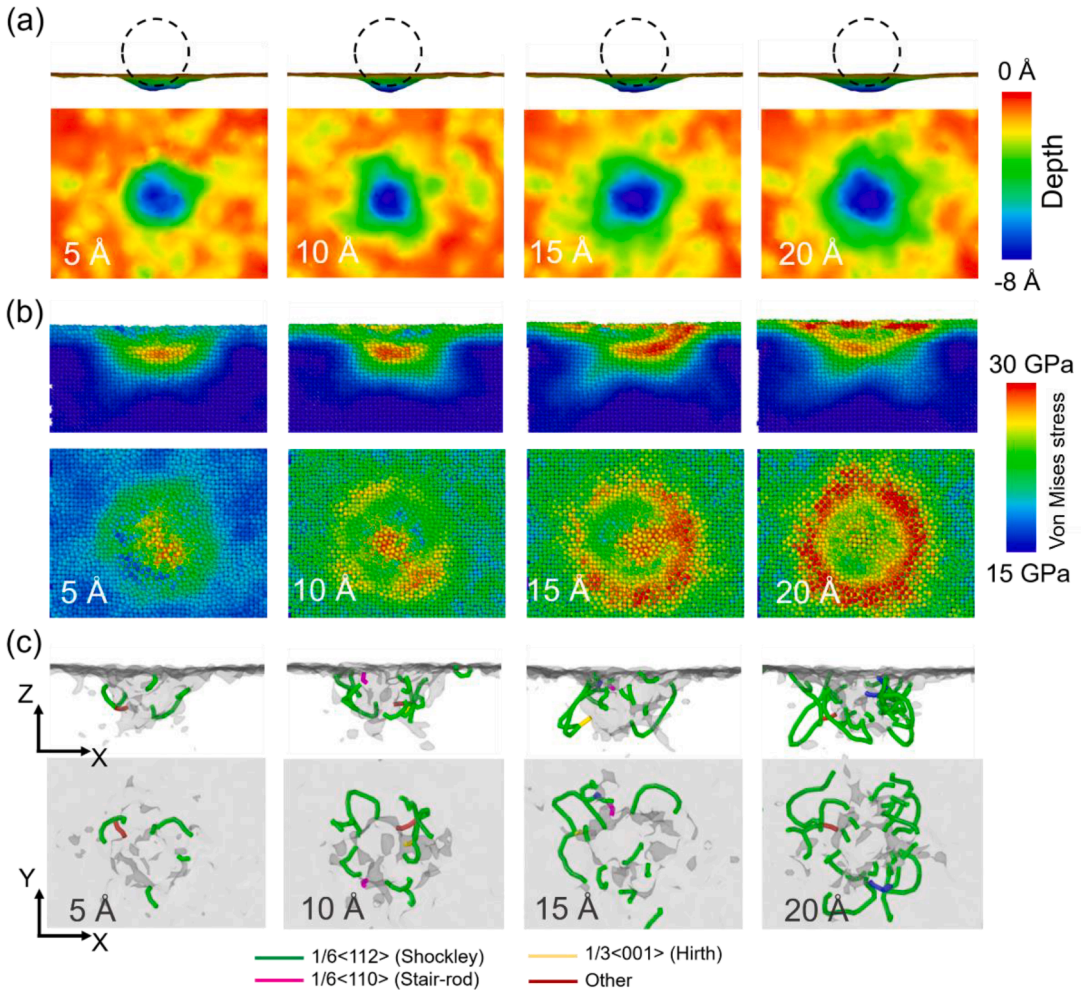

Fig. 11. (a) Contact surface morphology, (b) stress distribution, and (c) dislocation distribution within the work piece for various water film thicknesses during the indentation stage.

Considering the influence of the water film thickness on the passivation effect of the work piece surface, Fig. 12(c) further gives the number of passivated atoms for various water film thicknesses. It can be seen that the thicker the water film, the more obvious the passivation effect on the surface of the work piece, and the less likely the passivation effect is to be reduced. In addition, as shown in Fig. 12(c), the groove roughness in case of water-lubricated polishing is obviously smaller than that in case of dry polishing, and decreases with the increase of water film thickness, which agrees well with results in the literature [25].

Fig. 13(a) and (b) show the stress and dislocation distributions for various water film thicknesses at a polishing distance of 140 Å. It can be seen that with an increase in water film thickness, the stress on the work piece surface increases. The maximum stress region is arc-shaped at the front of the abrasive. Therefore, the dislocations are mainly concentrated below the indentation and the front of abrasive, and a small number of dislocations are distributed in the grooves, as shown in Fig. 13(b). When the water film thickness is 20 Å, a large number of dislocations accumulate at the indentation region. This is due to its larger indentation deformation region (see Fig. 11(a)) and greater stress concentration (see Fig. 11(b)), where the larger residual stress (see Fig. 13(a)) leads to the retention of dislocations. Fig. 13(c) shows the subsurface damage thickness and average dislocation length for various water film thicknesses. It can be seen that the average dislocation length increases monotonically, while the subsurface damage thickness decreases at first, but then increases with the water film thickness. Therefore, we may draw the conclusion that subsurface damage and groove surface quality are significantly improved by water-lubricated polishing, and that there exists a water film thickness allowing one to obtain optimal polishing quality. Thus, under CMP conditions, a moderate amount of polishing slurry is preferable to a large dose to ensure decent service performance of the work piece.

4. Conclusion

We have carried out an MD simulation study on the surface/subsurface damage mechanism in sliding and rolling abrasive polishing of Invar considering the effect of water. The main conclusions can be summarized as follows:

(1) A water-lubricated environment changes the interaction between the abrasive and the work piece atoms by passivating the work piece atoms with water molecules, which results in the improvement of wear resistance and surface quality. Water molecules change the stresses on the work piece surface, resulting in an uneven stress distribution. The stress concentration within the groove in dry polishing leads to greater subsurface damage than in water-lubricated environments.

(2) Under the same water film thickness, with an increase of abrasive rolling speed, the contact point between the abrasive and the work piece changes from the $+X$ direction to the $-X$ direction with respect to the abrasive position. The rolled-over work piece atoms transition from a forward motion to a reverse motion, and atomic accumulation occurs behind the abrasive. The higher the rolling speed, the more passivated atoms can be retained on the surface after polishing, resulting in better

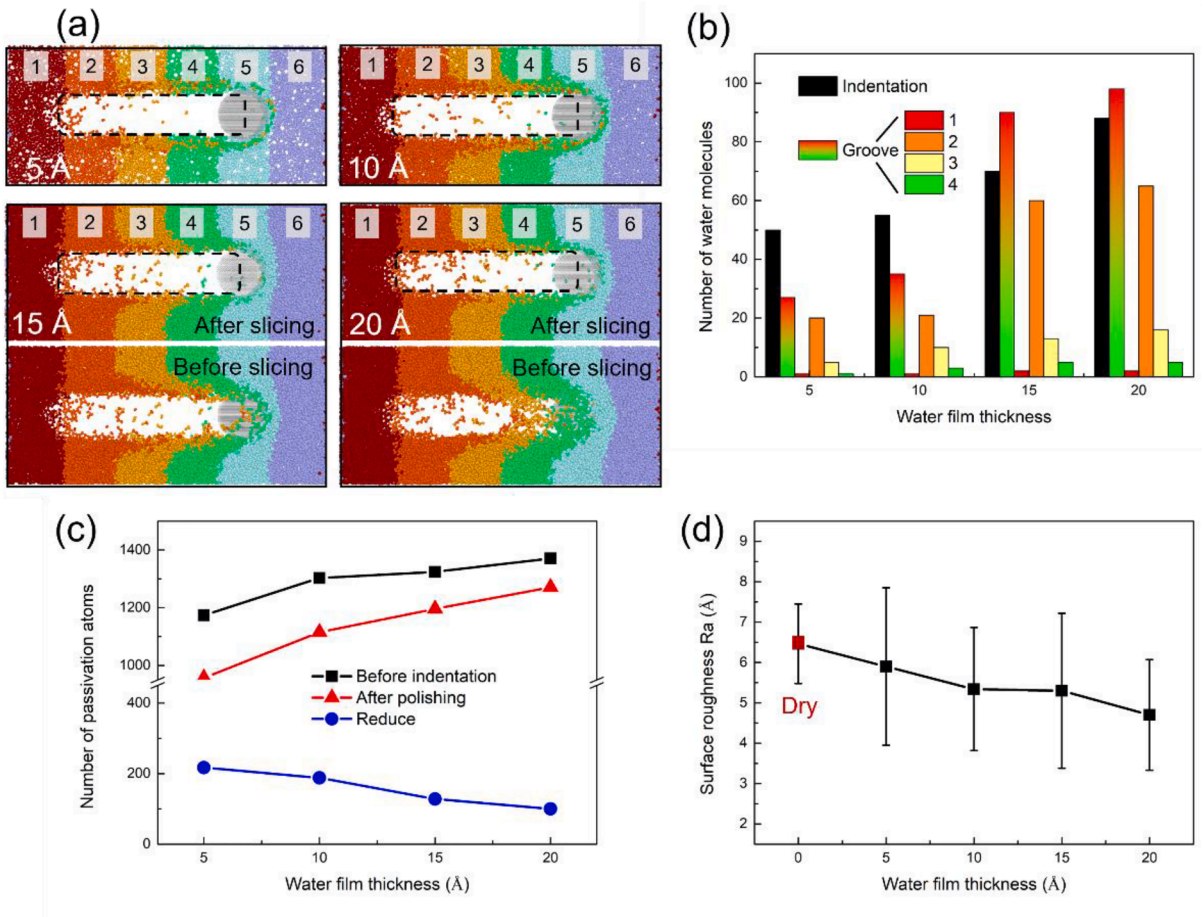

Fig. 12. (a) Distribution of water molecules in various regions (the water film is separated into several zones marked by different colors, and the movement of water molecules occurs in 6 zones marked by numbers 1–6. The black line marks the polishing contour. The work piece atoms are hidden for clarity.). (b) Number of water molecules below the indentation region and in the grooves, (c) Variations of passivated atoms and (d) surface roughness for various water film thicknesses ($\omega = 150$ m s^{-1}, $h = 5$ Å).

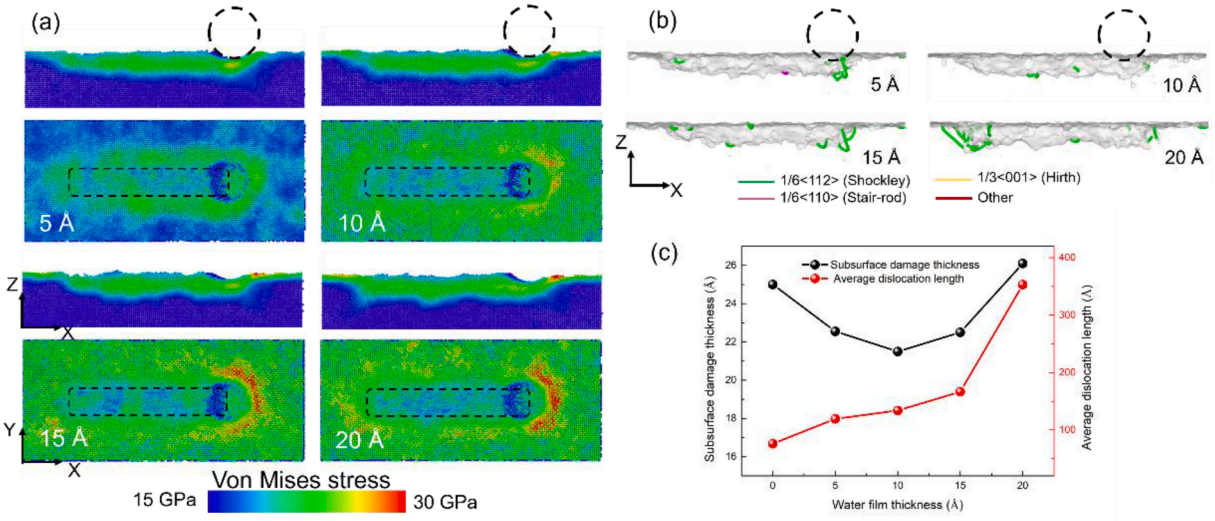

Fig. 13. (a) Von Mises stress distribution, (b) dislocation distribution, and (c) subsurface damage thickness and average dislocation length for various water film thicknesses at a polishing distance of 140 Å ($\omega = 150$ m s^{-1}, $h = 5$ Å).

surface quality. Under the combined influence of stress and movement form of the abrasive, the subsurface damage is greatest when the rolling speed is equal to the sliding speed.

(3) The thicker the water film, the stronger the passivation effect, which promotes the surface quality of the work piece. However, the thicker the water film, the greater the surface stress, which increases the subsurface damage thickness. Thus, in water-lubricated polishing, abrasives with a higher rolling speed and an appropriate amount of

water should be used to ensure a good balance between surface quality and microstructural integrity of the work piece.

CRediT authorship contribution statement

Wan Wang: Conceptualization, Methodology, Software, Writing – original draft, Writing – review & editing. **Dongpeng Hua:** Methodology, Investigation, Writing – original draft. **Qing Zhou:** Supervision, Resources, Funding acquisition, Writing – review & editing. **Shuo Li:** Investigation, Data curation. **Stefan J. Eder:** Supervision, Funding acquisition, Writing – review & editing. **Junqin Shi:** Supervision, Writing – review & editing. **Zhijun Wang:** Resources, Investigation, Data curation. **Haifeng Wang:** Supervision, Funding acquisition, Writing – review & editing. **Weimin Liu:** Writing – review & editing.

Declaration of Competing Interest

The authors declare that they have no known competing financial interests or personal relationships that could have appeared to influence the work reported in this paper.

Data availability

Data will be made available on request.

Acknowledgements

The authors would like to thank the Natural Science Foundation of China (no. 52175188), Key Research and Development Program of Shaanxi Province (2023-YBGY-434), State Key Laboratory for Mechanical Behavior of Materials (20222412) and the Fundamental Research Funds for the Central Universities (3102019JC001). SJE acknowledges financial support from the Austrian COMET-Program, Austria (Project K2 InTribology1, Grant No. 872176). Open access funding was provided by TU Wien (TUW).

References

[1] T.-Y. Kwon, M. Ramachandran, J.-G. Park, Scratch formation and its mechanism in chemical mechanical planarization (CMP), Friction 1 (2013) 279–305.
[2] R. Manivannan, S. Ramanathan, The effect of hydrogen peroxide on polishing removal rate in CMP with various abrasives, Appl. Surf. Sci. 255 (2009) 3764–3768.
[3] D. Zhao, X. Lu, Chemical mechanical polishing: Theory and experiment, Friction 1 (2013) 306–326.
[4] D. Datta, H. Rai, S. Singh, M. Srivastava, R.K. Sharma, N.N. Gosvami, Nanoscale tribological aspects of chemical mechanical polishing: a review, Appl. Surf. Sci. Adv. 11 (2022), 100286.
[5] Z.-C. Lin, R.-Y. Wang, S.-H. Ma, Theoretical model and experimental analysis of chemical mechanical polishing with the effect of slurry for abrasive removal depth and surface morphology of silicon wafer, Tribol. Int. 117 (2018) 119–130.
[6] Q. Zhai, W. Zhai, B. Gao, Y. Shi, X. Cheng, Effect of core-diameters and shell-thicknesses of Fe_3O_4/SiO_2 composite abrasives on the performance of ultrasound-assisted magnetorheological polishing for sapphire, Colloid. Surface. A 625 (2021), 126871.
[7] Z. Zhang, J. Cui, J. Zhang, D. Liu, Z. Yu, D. Guo, Environment friendly chemical mechanical polishing of copper, Appl. Surf. Sci. 467–468 (2019) 5–11.
[8] H. Lei, J. Luo, CMP of hard disk substrate using a colloidal SiO_2 slurry: preliminary experimental investigation, Wear 257 (2004) 461–470.
[9] X. Chen, Y. Zhao, Y. Wang, H. Zhou, Z. Ni, W. An, Nanoscale friction and wear properties of silicon wafer under different lubrication conditions, Appl. Surf. Sci. 282 (2013) 25–31.
[10] L. Liao, Z. Zhang, F. Meng, D. Liu, B. Wu, Y. Li, W. Xie, A novel slurry for chemical mechanical polishing of single crystal diamond, Appl. Surf. Sci. 564 (2021), 150431.
[11] Q. Luo, J. Lu, Z. Tian, F. Jiang, Controllable material removal behavior of 6H-SiC wafer in nanoscale polishing, Appl. Surf. Sci. 562 (2021), 150219.
[12] Q. Mu, Z. Jin, X. Han, Y. Yan, Z. Zhang, P. Zhou, Effects of slurry pH on chemical and mechanical actions during chemical mechanical polishing of YAG, Appl. Surf. Sci. 563 (2021), 150359.
[13] L. Wang, P. Zhou, Y. Yan, C. Hou, D. Guo, Micro-scale contact behavior and its effect on the material removal process during chemical mechanical polishing, Tribol. Int. 156 (2021), 106831.
[14] D. Luo, Q. Zhou, W. Ye, Y. Ren, C. Greiner, Y. He, H. Wang, Design and characterization of self-lubricating refractory high entropy alloy-based multilayered films, ACS Appl. Mater. Inter. 13 (2021) 55712–55725.
[15] Q. Zhou, D. Luo, D. Hua, W. Ye, S. Li, Q. Zou, Z. Chen, H. Wang, Design and characterization of metallic glass/graphene multilayer with excellent nanowear properties, Friction 10 (11) (2022) 1913–1926.
[16] K. Adachi, I.M. Hutchings, Wear-mode mapping for the micro-scale abrasion test, Wear 255 (2003) 23–29.
[17] Q. Zhang, J. Pan, X. Zhang, J. Lu, Q. Yan, Tribological behavior of 6H–SiC wafers in different chemical mechanical polishing slurries, Wear 472–473 (2021), 203649.
[18] J. Li, Q. Fang, L. Zhang, Y. Liu, Subsurface damage mechanism of high speed grinding process in single crystal silicon revealed by atomistic simulations, Appl. Surf. Sci. 324 (2015) 464–474.
[19] S.J. Eder, P.G. Grützmacher, T. Spenger, H. Heckes, H. Rojacz, A. Nevosad, F. Haas, Experimentally validated atomistic simulation of the effect of relevant grinding parameters on work piece topography, internal stresses, and microstructure, Friction 10 (2021) 608–629.
[20] J. Guo, S. Tan, C. Xiao, Atomistic understanding of scratching-induced material attrition of wurtzite single-crystal AlN using nanoscale diamond abrasive, Tribol. Int. 169 (2022), 107483.
[21] Z. Wu, L. Zhang, S. Yang, C. Wu, Effects of grain size and protrusion height on the surface integrity generation in the nanogrinding of 6H-SiC, Tribol. Int. 171 (2022), 107563.
[22] V.-T. Nguyen, T.-H. Fang, Molecular dynamics simulation of abrasive characteristics and interfaces in chemical mechanical polishing, Appl. Surf. Sci. 509 (2020), 144676.
[23] V.-T. Nguyen, T.-H. Fang, Abrasive mechanisms and interfacial mechanics of amorphous silicon carbide thin films in chemical-mechanical planarization, J. Alloys Compd. 845 (2020), 156100.
[24] V.-T. Nguyen, T.-H. Fang, Revealing the mechanisms for inactive rolling and wear behaviour on chemical mechanical planarization, Appl. Surf. Sci. 595 (2022), 153524.
[25] X. Meng, W. Wu, B. Liao, H. Dai, Atomic simulation of textured silicon carbide surface ultra-precision polishing, Ceram. Int. 48 (2022) 17034–17045.
[26] J. Shi, L. Fang, K. Sun, W. Peng, J. Ghen, M. Zhang, Surface removal of a copper thin film in an ultrathin water environment by a molecular dynamics study, Friction 8 (2019) 323–334.
[27] Y. Tian, H. Feng, J. Li, Q. Fang, L. Zhang, Nanoscale sliding friction behavior on Cu/Ag bilayers influenced by water film, Appl. Surf. Sci. 545 (2021), 148957.
[28] Y. Li, M. Lai, F. Fang, Effects of polishing speed and a water environment on the mechanism of nanometric mechanical polishing of single-crystal lutetium oxide, Mater. Today Commun. 30 (2022), 103194.
[29] C.E. Guillaume, Invar and its applications, Nature 71 (1904) 134–139.
[30] A. Sahoo, V.R.R. Medicherla, Fe-Ni invar alloys: a review, Mater. Today: Proc. 43 (2021) 2242–2244.
[31] M. van Schilfgaarde, I.A. Abrikosov, B. Johansson, Origin of the Invar effect in iron–nickel alloys, Nature 400 (1999) 46–49.
[32] Z. Wang, J. Li, Q. Fang, B. Liu, L. Zhang, Investigation into nanoscratching mechanical response of AlCrCuFeNi high-entropy alloys using atomic simulations, Appl. Surf. Sci. 416 (2017) 470–481.
[33] W. Wang, D. Hua, D. Luo, Q. Zhou, S.J. Eder, S. Li, Z. Wang, H. Wang, Exploring the nano-polishing mechanisms of Invar, Tribol. Int. 175 (2022), 107840.
[34] C. Wu, B.-J. Lee, X. Su, Modified embedded-atom interatomic potential for Fe-Ni, Cr-Ni and Fe-Cr-Ni systems, Calphad 57 (2017) 98–106.
[35] M.F. Dopke, O.A. Moultos, R. Hartkamp, On the transferability of ion parameters to the TIP4P/2005 water model using molecular dynamics simulations, J. Chem. Phys. 152 (2020), 024501.
[36] J. Liu, Q. Zhen, C.J. Zhao, L.U. Wen-Qiang, Corrosion study of iron in liquid lead-bismuth eutectic in accelerator driven system by molecular dynamics method, J. Eng. Thermophys. 38 (2017) 557–561.
[37] Y. Gao, C.J. Ruestes, H.M. Urbassek, Nanoindentation and nanoscratching of iron: Atomistic simulation of dislocation generation and reactions, Comput. Mater. Sci. 90 (2014) 232–240.
[38] J. Shi, J. Chen, L. Fang, K. Sun, J. Sun, J. Han, Atomistic scale nanoscratching behavior of monocrystalline Cu influenced by water film in CMP process, Appl. Surf. Sci. 435 (2018) 983–992.
[39] D. Zhang, Z.-M. Bi, H.-L. Sun, L. Cheng, Y.-X. Liu, Z.-Y. Hu, B. Wang, High-temperature oxidation mechanism of Fe-3.0wt%Si electrical steel with hybrid atmosphere, J. Alloys Compd. 913 (2022), 165247.
[40] S. Min, H. Liu, J. Wang, J. Hou, Early oxidation behavior of Ni-based Alloy 690 in simulated pressurized water reactor environment with varying surface conditions, Corros. Commu. 4 (2021) 68–81.
[41] F. Gandomi, M. Vakili, V. Darugar, R. Takjoo, S.F. Tayyari, Optimized molecular geometry, vibrational analysis, and Fe-O bond strength of Tris (α-cyanoacetylacetonate)iron(III): An experimental and theoretical study, J. Mol. Struct. 1248 (2022), 131444.
[42] I.G. Shuttleworth, Bond length effects during the dissociation of O_2 on Ni(1 1 1), Appl. Surf. Sci. 346 (2015) 329–334.
[43] C. Li, W. Tang, X.-Z. Tang, L. Yang, L. Bai, A molecular dynamics study on the synergistic lubrication mechanisms of graphene/water-based lubricant systems, Tribol. Int. 167 (2022), 107356.
[44] A. Stukowski, Visualization and analysis of atomistic simulation data with OVITO–the Open Visualization Tool, Model. Simul. Mater. Sc. 18 (2009), 015012.
[45] A. Stukowski, K. Albe, Extracting dislocations and non-dislocation crystal defects from atomistic simulation data, Model. Simul. Mater. Sc. 18 (2010), 085001.

[46] Q. Jia, W. He, D. Hua, Q. Zhou, Y. Du, Y. Ren, Z. Lu, H. Wang, F. Zhou, J. Wang, Effects of structure relaxation and surface oxidation on nanoscopic wear behaviors of metallic glass, Acta Mater. 232 (2022), 117934.
[47] Y. Qi, J. Liu, Y. Dong, X.-Q. Feng, Q. Li, Impacts of environments on nanoscale wear behavior of graphene: Edge passivation vs. substrate pinning, Carbon 139 (2018) 59–66.
[48] Z. Wu, L. Zhang, S. Yang, Effect of abrasive grain position patterns on the deformation of 6H-silicon carbide subjected to nano-grinding, Int. J. Mech. Sci. 211 (2021), 106779.
[49] P. Zhou, J. Li, Z. Wang, J. Chen, X. Li, Y. Zhu, Molecular dynamics study of the removal mechanism of SiC in a fixed abrasive polishing in water lubrication, Ceram. Int. 46 (2020) 24961–24974.
[50] J. Li, Q. Fang, L. Zhang, Y. Liu, The effect of rough surface on nanoscale high speed grinding by a molecular dynamics simulation, Comput. Mater. Sci. 98 (2015) 252–262.
[51] M.B. Cai, X.P. Li, M. Rahman, Study of the temperature and stress in nanoscale ductile mode cutting of silicon using molecular dynamics simulation, J. Mater. Process. Tech. 192–193 (2007) 607–612.
[52] V.T. Nguyen, T.H. Fang, Phase transformation and subsurface damage formation in the ultrafine machining process of a diamond substrate through atomistic simulation, Sci. Rep. 11 (2021) 17795.
[53] Y. Zhou, Y. Huang, J. Li, F. Zhu, Effect of water film on the nano-scratching process of 4H-SiC under the constant load, Tribol. Int. 175 (2022), 107802.
[54] J. Ren, J. Zhao, Z. Dong, P. Liu, Molecular dynamics study on the mechanism of AFM-based nanoscratching process with water-layer lubrication, Appl. Surf. Sci. 346 (2015) 84–98.
[55] J. He, J. Sun, Y. Meng, Y. Pei, P. Wu, Synergistic lubrication effect of Al_2O_3 and MoS_2 nanoparticles confined between iron surfaces: a molecular dynamics study, J. Mater. Sci. 56 (2021) 9227–9241.
[56] D. Hua, W. Wang, D. Luo, Q. Zhou, S. Li, J. Shi, M. Fu, H. Wang, Molecular dynamics simulation of the tribological performance of amorphous/amorphous nano-laminates, J. Mater. Sci. Tech. 105 (2022) 226–236.
[57] J. Shi, J. Chen, X. Wei, L. Fang, K. Sun, J. Sun, J. Han, Influence of normal load on the three-body abrasion behaviour of monocrystalline silicon with ellipsoidal particle, RSC Adv. 7 (2017) 30929–30940.
[58] S. Huang, H. Wu, Z. Jiang, H. Huang, Water-based nanosuspensions: Formulation, tribological property, lubrication mechanism, and applications, J. Manuf. Process. 71 (2021) 625–644.
[59] W. Xie, F. Fang, Mechanism of atomic and close-to-atomic scale cutting of monocrystalline copper, Appl. Surf. Sci. 503 (2020), 144239.
[60] H. Wang, Z. Dong, S. Yuan, X. Guo, R. Kang, Y. Bao, Effects of tool geometry on tungsten removal behavior during nano-cutting, Int. J. Mech. Sci. 107384 (2022).
[61] B. Zhao, Y. Zhang, Y. Fan, X. Yu, Z. Zhang, B. Zhang, The three-body abrasive tribological characteristics of the Graphene/h-BN heterostructure film considering defects, Tribol. Int. 171 (2022), 107525.
[62] W. Wang, D. Hua, D. Luo, Q. Zhou, S. Li, J. Shi, H. Wang, Molecular dynamics simulation of deformation mechanism of CoCrNi medium entropy alloy during nanoscratching, Comput. Mater. Sci. 203 (2022), 111085.
[63] A. Opitz, S.-U. Ahmed, J. Schaefer, M. Scherge, Friction of thin water films: a nanotribological study, Surf. Sci. 504 (2002) 199–207.
[64] V. Bhardwaj, Q. Zhou, F. Zhang, W. Han, Y. Du, K. Hua, H. Wang, Effect of Al addition on the microstructure, mechanical and wear properties of TiZrNbHf refractory high entropy alloys, Tribol. Int. 160 (2021), 107031.
[65] X. Liu, D. Hua, W. Wang, Q. Zhou, S. Li, J. Shi, Y. He, H. Wang, Atomistic understanding of incipient plasticity in BCC refractory high entropy alloys, J. Alloys Compd. 920 (2022), 166085.